Modulation Limit Based Control Strategy for More Electric Aircraft Generator System

Author, co-author (Do NOT enter this information. It will be pulled from participant tab in MyTechZone)

Affiliation (Do NOT enter this information. It will be pulled from participant tab in MyTechZone)

Abstract

Vector based control strategies have been extensively employed for drive systems, and in recent times to the More Electric Aircraft (MEA) generator based systems. The control schemes should maintain the bus voltage and adhere to the generator system voltage and current limits throughout a wide speed range. Typically, the current limit is prioritised first due to ease of implementation and simple control structure. As a result, the voltage limit can be exceeded due to change in operating conditions or disturbance factors. In flux weakening regions, this may affect the controllability of the power converter and lead to generator system instability. In this paper, an alternative control strategy has been investigated to address this drawback. The proposed control scheme refers to the modulation index limit which is the ratio between the power converter input and output voltages as the voltage limit. The control scheme uses a dynamic limit for the generator reference voltages such that the modulation index limit is adhered. Furthermore, a controller is introduced to address the lack of current limit of the proposed control scheme. The linear open loop plant is derived for the bus voltage and current limit controllers and verified against their equivalent non-linear counterparts. They are used to evaluate and design the controllers for stable operation. The performance of the proposed control scheme is then compared with a state of the art existing control method. Simulation results showed superior modulation index limit throughout and short duration stator current overshoots when operating at current limit. Overall, the proposed control strategy showed to be a suitable alternative control scheme for the MEA generator system.

Introduction

The more electric aircraft (MEA) trend has been gaining traction through enabling technologies from power electronics and electrical machines. This initiative aims to increase the reliance on electrical power on-board aircraft for load applications that have been traditionally been powered by pneumatic, hydraulic, or mechanical power. Such changes within the aircraft may offer benefits in terms of design, prognostics, and efficiency [1, 2].

As such, the electrical power generation system would have to undergo significant changes in the categories of power output density, power rating, and reliability to supply the increase in load demand [3]. The core modification is the exclusion of constant frequency gearbox commonly used in civil aircraft which allows a more direct interface engine connection to the electrical generator. The electrical power generated which is variable frequency (VF) with respect to engine speed can then be regulated using power electronic converters. Various machine-converter configurations have been explored in [4] and a very promising topology for future aircraft generator system is based on permanent magnet machine (PMM) with bidirectional converter as depicted in Figure 1.
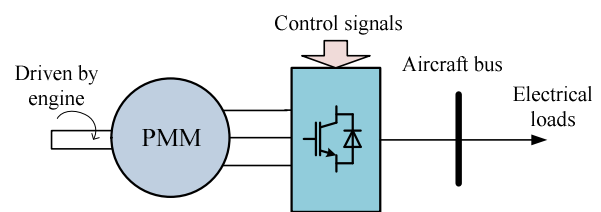

Figure 1. Power generator system configuration.

There are various control functions that should be undertaken by the generator system. Among the tasks is bus voltage control (typically 270V for high voltage DC buses) to ensure that the electrical loads can operate nominally. Another task is to ensure that the current does not exceed the converter ratings limit. Flux weakening may be considered to maintain generator controllability when operating in high speed regions (up to 30,000rpm). De-fluxing current is injected into the machine in order to reduce the machine back-emf and maintain the modulation index ratio, m [5]. This ratio relates to the input and output converter voltages and hence be considered the voltage limit.

Literature covering the controller design for the MEA generator systems has been covered in [5], [6], and [7]. The control schemes in the quoted literature were designed to accomplish the functionalities stated earlier, however the m limit, is not strictly obeyed. Due to the control structure that will be discussed in the following Section, the current limit is prioritised first which allows some room for variation in the voltage. In flux weakening region where m has to be strictly obeyed, the variation may cause uncontrolled instances that can affect the generators controllability [8]. If the limit is breached, the control signals cannot be correctly applied by the power converter and thus the generator will operate at inaccurate voltage levels. This problem can be mitigated by setting a safe margin for the m limit, however at the cost of converter performance.

09/25/2018

In this paper, an alternative control scheme is introduced where the *m* limit is prioritised in order to ensure controllability of the generator system. The proposed control also takes into account the bus voltage regulation and current limit protection. The content is structured as follows; a state of the art aircraft generator control structure and the proposed control strategy are introduced, followed by controller design analysis of the latter. Then, the comparison results between the two control schemes are discussed and conclusion are made at the end of the paper.

Control Schemes

The power system shown in Figure 1 is used as the power generator system for this investigation. The converter considered is an active front end which converts AC to DC power for a high voltage DC bus network. The general structure of the control scheme presented in the mentioned literature can be seen in Figure 2. i_{dq} and v_{dq} are the stator currents and voltages in the rotating reference dq frame respectively. L_{dq} are the PMM inductances in dq frame, ω_e is the electrical speed, ψ_m is the PMM flux, $|v_s|$ is the stator voltage magnitude, E_{dc} is the DC bus voltage, m_{dq} and m_{abc} are the modulation indexes in dq and three phase frame respectively. k_s is the ratio between the AC and DC voltages depending on the pulse width modulation scheme. i_{slim} and i_{qlim} are the stator current and i_q limits respectively.

The cascaded control structure consists of the inner and outer control loop. The inner loop serves to regulate i_d and i_q based on their reference signals from the outer loop. The outer loop is set to control $|v_s|$ for flux weakening and E_{dc}. $|v_s|$ is controlled based on the following voltage limit:

$$|v_{s\,\lim}| \geq \sqrt{v_d^{*2} + v_q^{*2}} \qquad (1)$$

where $|v_{slim}|$ is the stator voltage limit. The voltage limit can be interpreted in terms of *m* using the AC and DC voltages:

$$m_{\lim} \geq \sqrt{m_d^{\,2} + m_q^{\,2}} \qquad (2)$$

$$m_d = \frac{v_d^{\,*}}{E_{dc}k_s}, m_q = \frac{v_q^{\,*}}{E_{dc}k_s} \qquad (3)$$

where $m_{\lim}$ is the modulation index limit. *m* can be compared with high frequency carrier signals to be translated into pulses for the power converter switches with pulse width modulation. Typically, the amplitude of *m* should be less than one to achieve the desired modulation of the control signals into converter voltages. However, when *m* is more than one, the comparison process is partially modulated as the signals are saturated. The output voltages becomes inaccurate and the operating mode differs from what the control intends. For this study, $m_{\lim}$ is set to 1 to enable full use of the available voltage and to simplify comparison with the proposed control scheme [8]. The current limit for this control method can be set with a dynamic limit at the output of E_{dc} controller that obeys:

$$i_{s\,\lim} \geq \sqrt{i_d^{\,2} + i_q^{\,2}} \qquad (4)$$

The limit is set on the *q*-axis loop to provide flux weakening priority over E_{dc} control. Overall, the structure enables voltage and current limits through the $|v_s|$ controller and the dynamic limit respectively. This control scheme has been extensively covered in [5, 9, 10] and notably, it has been reported that the $|v_s|$ controller has some stability limits and hence is needed to be designed carefully. The current is limited by the dynamic limit and there is a potential to exceed the *m* limit (2) due to the $|v_s|$ controller error corrective action. Hence, this control method is referred as the current limit control scheme.

Figure 3 shows the proposed control scheme that prioritises voltage limitation instead of current. A dynamic limit is used on the *d*-axis loop that takes into account equation (2) in order to enable flux weakening in this control scheme. When $m_{\lim}$ is reached, i.e., within flux weakening region, the *q*-axis control loop shall determine the value for m_d which then introduces i_d as the reactive current to de-flux the PMM. Outside the flux weakening region, i_d is controlled to zero as it is not required. The inner loop controllers are similar to the ones in the current limit control scheme.

The outer control loop consists of two controllers for E_{dc} and i_s located on the *q*-axis. The i_s controller is present as there is a lack of current restrictions present within the control scheme. When i_s exceeds its reference value, i_{q2}^* reduces in order to meet the current limit (4). The output of these controllers can be used to determine i_q^*. The two signals are compared using a minimum function and the smallest value at a given time is selected as i_q^*. The minimum function is used as it is assumed that the power flow from the PMM to the DC bus is negative, hence i_q is mainly negative. Back tracing (BT) is also used to maintain similar integrator states between the outer loop controllers [11]. This algorithm maintains all of the controllers' integrator states to be of similar value with respect to output i_q^*.

Control Design and Analysis

The control plants are derived for the proposed control scheme in this Section to help with the outer loop controller design. Compared to the initial control scheme, the flux weakening controller does not need to be designed as it is inherently controlled by the dynamic limit. The plant of E_{dc} and i_s should be derived. The stability analysis is performed in small signal domain which only considers linear plants. The non-linear elements of the equations are linearised around a given operating point to obtain the linear plants. The parameters used are located in the Appendix Section. The following are the key linear equations used to derive the necessary plants. General equations of PMM are used ((5) and (6)) to allow consideration towards both salient and non-salient type PMMs.

$$\Delta v_d = R_s \Delta i_d + L_d s \Delta i_d - L_q \omega_{eo} \Delta i_q \qquad (5)$$

$$\Delta v_q = R_s \Delta i_q + L_q s \Delta i_q + L_d \omega_{eo} \Delta i_d \qquad (6)$$

$$\Delta i_{dc} = \begin{bmatrix} -\dfrac{3}{2E_{dco}}(v_{do}\Delta i_d + i_{do}\Delta v_d + v_{qo}\Delta i_q + i_{qo}\Delta v_q) \\[4mm] +\dfrac{3}{2E_{dco}^{\,2}}(v_{do}i_{do} + v_{qo}i_{qo})\Delta E_{dc} \end{bmatrix} \qquad (7)$$
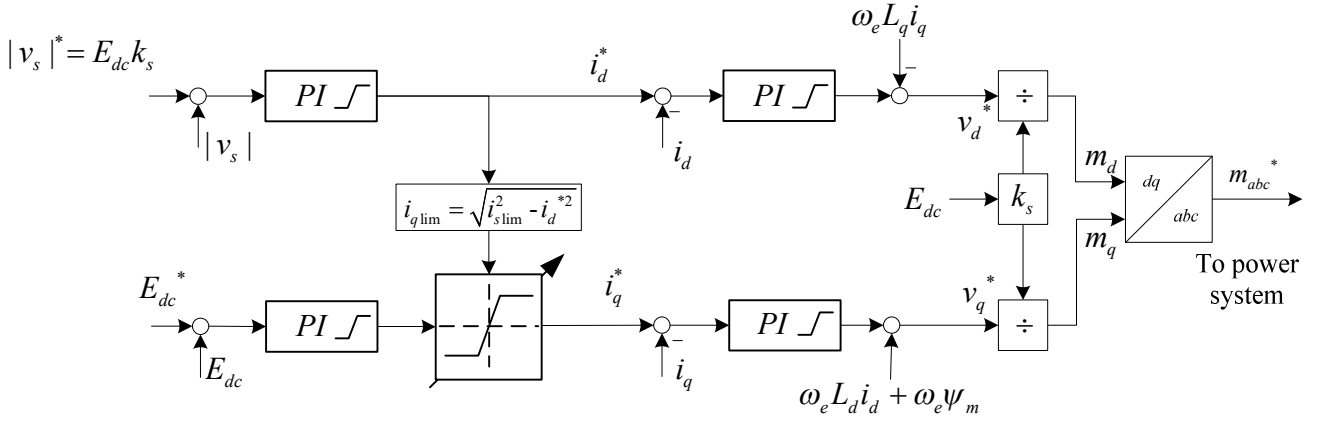
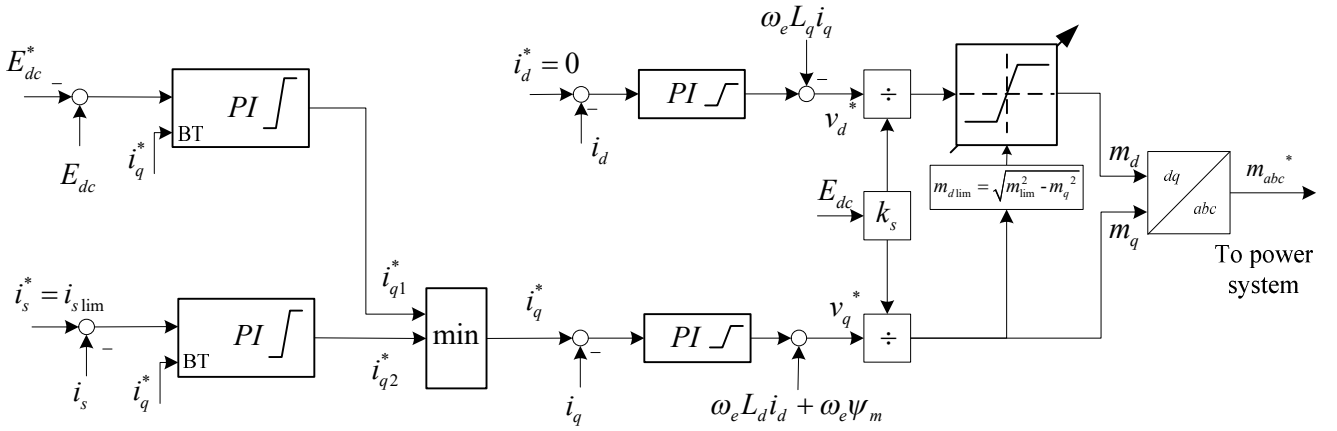Figure 2. Current limit based control strategy for MEA generator system.

Figure 3. Proposed modulation index limit control scheme.

$$\Delta E_{dc} = \frac{R_L}{CR_L s + 1} \Delta i_{dc} \qquad (8)$$

$$\Delta i_s = \frac{i_{do}}{i_{so}} \Delta i_d + \frac{i_{qo}}{i_{so}} \Delta i_q \qquad (9)$$

$$m_{do} \Delta m_d = -m_{qo} \Delta m_q \qquad (10)$$

$$\Delta v_d = k_s m_{do} \Delta E_{dc} + k_s E_{dco} \Delta m_d \qquad (11)$$

$$\Delta v_q = k_s m_{qo} \Delta E_{dc} + k_s E_{dco} \Delta m_q \qquad (12)$$

It was found that the mechanical model does not affect the plant significantly. Hence, ω_e is assumed to be constant in order to simplify the derived plant. The inner current loop design has been discussed in [12] and the controller has been designed to achieve 500Hz bandwidth. The closed loop transfer function for i_q is:

$$\frac{\Delta i_q}{\Delta i_q^{*}} = \frac{k_{pq}s + k_{iq}}{L_q s^2 + (R_s + k_{pq})s + k_{iq}} \qquad (13)$$

where k_{pq} and k_{iq} are the proportional and integral terms of i_q controller.

E_{dc} Control Loop

The plant for this control loop should relate input Δi_q^{*} to output ΔE_{dc}. Using equation (7), each small signal term can be replaced with the other linear equations so that the plant can be found as:

$$\frac{\Delta E_{dc}}{\Delta i_q^{*}} = \frac{-3E_{dco}R_L(x_1 s^2 + x_2 s + x_3)}{(y_1 s^2 + y_2 s + y_3)} \frac{\Delta i_q}{\Delta i_q^{*}} \qquad (14)$$
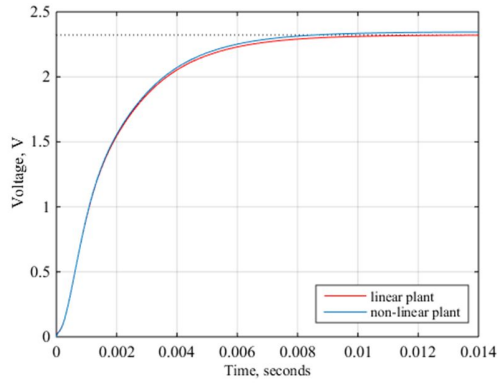
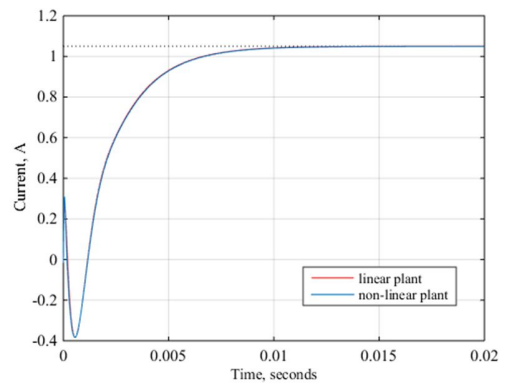Figure 4. E_{dc} step response comparison to i_q^*=1A.

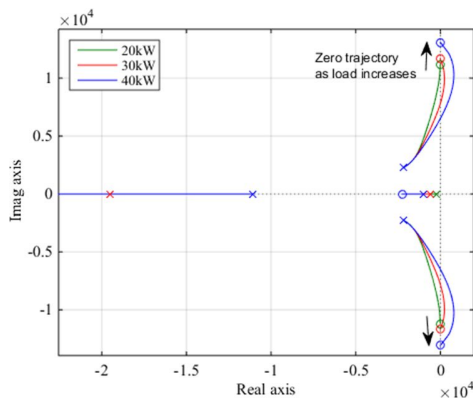Figure 7. i_s step response comparison to i_q^*=1A.

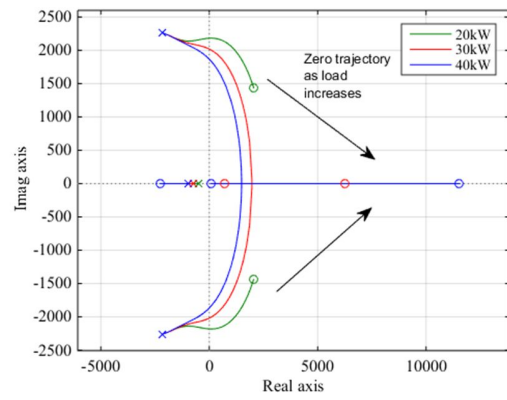Figure 5. E_{dc} open loop root locus at various loads.

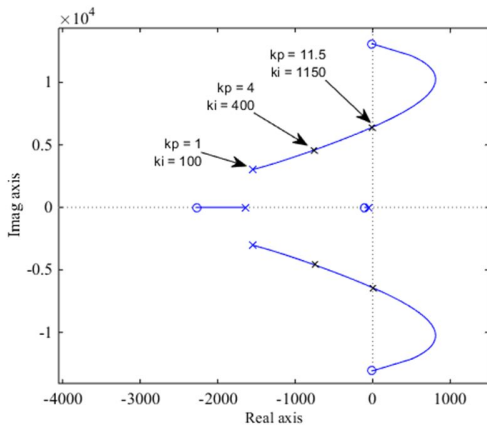Figure 8. i_s open loop root locus at various loads.
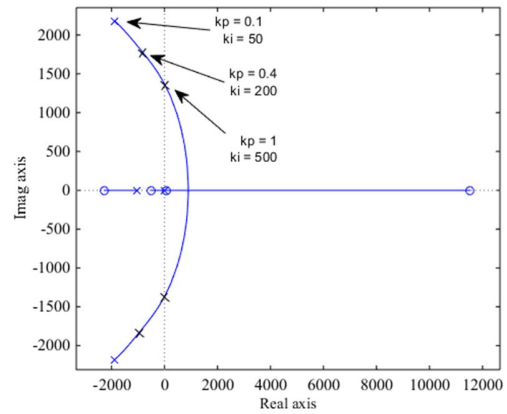

Figure 6. E_{dc} closed loop root locus.

Figure 9. i_s closed loop root locus.

The coefficients for x_1, x_2, x_3, y_1, y_2, and y_3 are located in the Appendix section. This linear plant is verified with an equivalent non-linear model built in Simulink via step response comparison as seen in Figure 4. The open loop root locus at different loads were also plotted as depicted in Figure 5. As the load power increases, there is a tendency for the conjugate zeroes to move closer to the imaginary axis. This results in pole trajectories that lie on the right half plane

which may cause instability when the closed loop gain is within that region. Therefore, the plant at full load should be considered for the control design to take into account the unstable region. The closed loop gain margin before instability can be seen in Figure 6. As long as the controller gain is selected to be within the gain margin, stability is ensured.

09/25/2018

i_s control loop

Since the stator current is the control variable for this loop, hence the plant can be derived from the linearised current limit equation (9). Using the equations (5) to (13), the i_s plant can be derived to be:

$$\frac{\Delta i_s}{\Delta i_q^*} = \frac{x_4 s^2 + x_5 s + x_6}{i_{so}(y_4 s^2 + y_5 s + y_6)} \frac{\Delta i_q}{\Delta i_q^*} \quad (15)$$

Similar to the previous analysis, plant is verified by step response comparison with the non-linear equivalent model as seen in Figure 7. The open loop root locus for this plant has been shown in Figure 8 for operating loads up to 40kW. There are zeroes on the right half plane which indicates non-minimum phase. There is a tendency for instability when the closed loop poles move towards the zeroes on the right half plane. The gain margin can be seen in Figure 9 at the highest load point and the controller should be selected such that its gains are within the margin.

Based on the analysis in this Section, both E_{dc} and i_s plants have gain margins for stable operation and their controllers should be designed carefully. The selection of full load operating point for small signal analysis can help with the control design process. The following gains have been selected for the outer loop controllers to achieve reasonable bandwidth response within the stable margins and they are shown in the Appendix Section. The back-tracing gains for the outer loop control have been selected as 150 for fast tracking during changes of controller output.

Simulation Results

Results showing comparison between both control methods are displayed and discussed in this Section. E_{dc}, flux weakening, and i_s regulation are demonstrated for both control schemes and compared with one another. The operating points were selected such that the operation of each outer loop controllers are distinct. The simulation started with $m_{lim} = 1$, $k_s = 1/\text{sqrt}(3)$, $E_{dc}^* = 270V$, and $i_{slim} = 155A$.

Figure 10 shows the E_{dc} regulation performance between the two control schemes when subjected to a resistive load, R_L, of 10kW step changes. Their PI controller values were selected to be the same and it can be seen that they respond well to the load changes with no difference between them. On the other hand, the voltage transients comply with MIL-STD-704F for a 270VDC power system [13].

The flux weakening control performance between both control schemes can be seen in Figure 11. The speed is varied from 10krpm to 20krpm to show operation in and out of flux weakening region. Then R_L is added at 10kW step while the power system is operating in flux weakening region. Flux weakening is shown to be active when i_d is non-zero. The m for current limit control scheme was observed to have a slight overshoot when the speed continues to 20krpm. As a result, the power system goes unstable as indicated by the increased E_{dc} in the same figure. The m limit control on the other hand does not exhibit such transient behaviours and m is always constrained to be within m_{lim}.

Figure 12 depicts the i_s regulation for both control strategies. It is assumed that i_{slim} is soft constrained and the generator system has sufficient power for the load if necessary. A step change of 10kW for P_L was applied for $i_s > i_{slim}$. The m limit control showed current
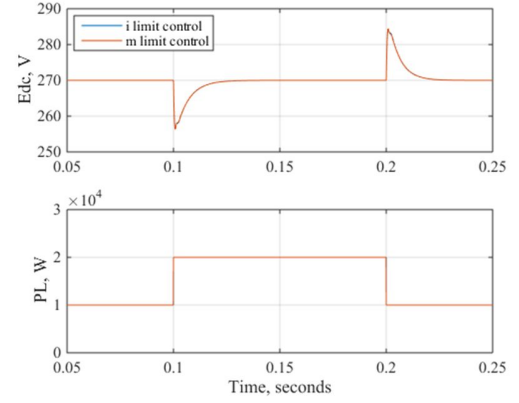

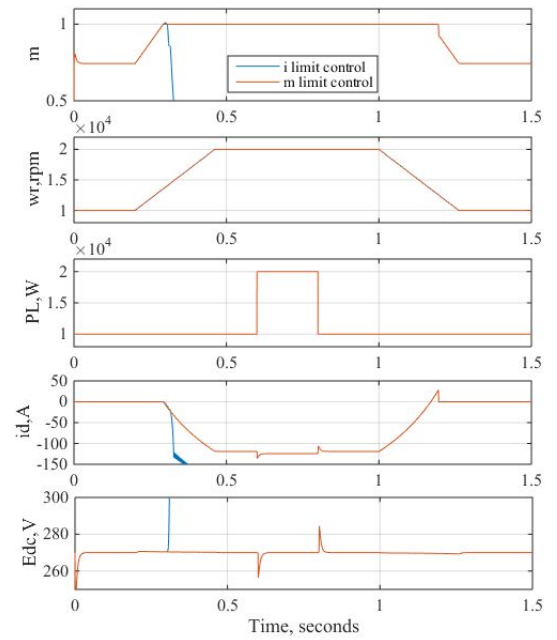Figure 10. Comparison between the two control schemes on E_{dc} control.

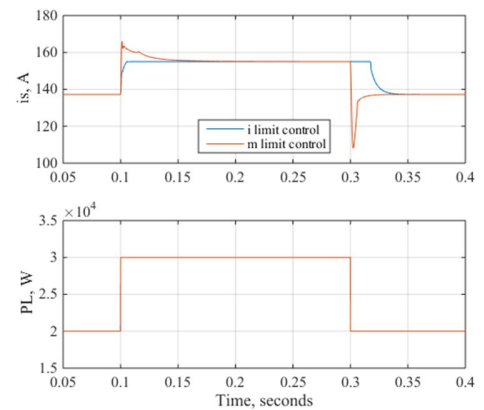Figure 11. Comparison between the two control schemes on flux weakening control.

Figure 12. Comparison between the two control schemes on i_s control.

09/25/2018

overshoot which is eventually regulated to i_{slim}. When P_L is reverted back to 10kW, different transients were observed for both control schemes. For the current limit control scheme, this is due to E_{dc} re-regulated to E_{dc}^* as there was insufficient i_q. As for the m limit control scheme, the dynamic transient of i_s comes from the E_{dc} controller which was selected by the minimum function as $i_s < i_{slim}$.

Overall, the m limit control achieves its aim to provide prioritised voltage regulation compared to the current limit control. The trade-off is that the m limit control allows current overshoot past i_{slim} which can be acceptable for short periods of time. On the other hand, the need to design a i_s controller is compensated by the simplified flux weakening control.

Conclusion

An alternative control scheme has been proposed in this paper for MEA generator systems. This control scheme prioritises voltage limitation to ensure generator controllability particularly in the flux weakening region. In addition to that, an i_s controller is added to address the lack of current limit in the proposed control scheme. The small signal plants have been derived to aid with the outer loop controller design process. The zero locations of the plants causes the pole trajectories towards the right half plane, which can cause instability if the controllers are not designed properly. The controllers should be designed at generator full load rating to guarantee stable operation. A state of the art control strategy has been used as a comparison for the three main control functionalities (E_{dc}, modulation index, and current limit). The proposed control scheme showed better voltage limit performance with the trade-off of short duration current overshoot. Experimental validation and further stability analysis with this control scheme are planned for upcoming works. Compliance of the control limit with aircraft standards shall also be looked at in future studies.

References

[1]   P. Wheeler and S. Bozhko, "The More Electric Aircraft: Technology and challenges," *Electrification Magazine, IEEE,* vol. 2, pp. 6-12, 2014.

[2]   X. Roboam, B. Sareni, and A. D. Andrade, "More Electricity in the Air: Toward Optimized Electrical Networks Embedded in More-Electrical Aircraft," *Industrial Electronics Magazine, IEEE,* vol. 6, pp. 6-17, 2012.

[3]   I. Moir and A. Seabridge, *Aircraft Systems: Mechanical, Electrical and Avionics Subsystems Integration*: Wiley, 2008.

[4]   A. Abdel-Hafez, *Power Generation and Distribution System for a More Electric Aircraft - A Review, Recent Advances in Aircraft Technology*, 2012.

[5]   S. S. Yeoh, F. Gao, S. Bozhko, and G. Asher, "Control design for PMM-based starter generator system for More Electric Aircraft," in *Power Electronics and Applications (EPE'14-ECCE Europe)*, 2014, pp. 1-10.

[6]   Y. Xibo and W. Jiabin, "Stability and performance analysis of permanent magnet motors operating in flux-weakening region," in *Power Electronics and Motion Control Conference (IPEMC), 2012 7th International*, 2012, pp. 2542-2546.

[7]   F. Gao, S. Bozhko, A. Costabeber, G. Asher, and P. Wheeler, "Control Design and Voltage Stability Analysis of a Droop-Controlled Electrical Power System for More Electric Aircraft," *IEEE Transactions on Industrial Electronics,* vol. 64, pp. 9271-9281, 2017.

[8]   A. Yazdani and R. Iravani, *Voltage-Sourced Converters in Power Systems*: John Wiley & Sons, Inc., 2010.

[9]   M. Yin, S. Bozhko, and S. S. Yeoh, "Control Design for PMM-Based Generator Fed by Active Front-End Rectifier in More-Electric Aircraft," *SAE Int. J. Aerosp.,* vol. 9, pp. 23-29, 2016.

[10]   S. Bozhko, S. S. Yeoh, F. Gao, and C. Hill, "Aircraft starter-generator system based on permanent-magnet machine fed by active front-end rectifier," in *Industrial Electronics Society (IECON)*, 2014, pp. 2958-2964.

[11]   H. B. Enalou and E. A. Soreshjani, "A Detailed Governor-Turbine Model for Heavy-Duty Gas Turbines With a Careful Scrutiny of Governor Features," *IEEE Transactions on Power Systems,* vol. 30, pp. 1435-1441, 2015.

[12]   P. C. Krause, O. Wasynczuk, S. D. Sudhoff, and I. P. E. Society, *Analysis of electric machinery and drive systems*: IEEE Press, 2002.

[13]   "MIL-STD-704F," in *Aircraft Electric Power Characteristics*, ed. United States of America: Department of Defense Interface Standard, 2014.

09/25/2018

Appendix

Power system parameters

Parameter	Variable	Value
Machine rated power	P_{rated}	40kW
Machine rated speed	ω_r	20,000rpm
Machine rated current	i_{rated}	170A
Stator resistance	R_s	1.058mΩ
d-axis stator inductance	L_d	99µH
q-axis stator inductance	L_q	99µH
Magnet flux	ψ_m	0.03644Wb
Pole pairs	p	3
DC bus capacitance	C	1.2mF
Inner loop PI controller gains	k_p, k_i	0.43, 977
Outer loop E_{dc} controller gains	k_{pe}, k_{ie}	1.5, 300
Outer loop i_s controller gains	k_{pi}, k_{ii}	0.5, 200

Plant Coefficients

$$x_1 = L_d L_q \left(i_{qo} m_{do} - i_{do} m_{qo} \right)$$

$$x_2 = R_s i_{qo} m_{do} \left(L_d + L_q \right) - R_s i_{do} m_{qo} \left(L_d + L_q \right) - L_q m_{qo} v_{do} + L_d m_{do} v_{qo}$$

$$x_3 = -R_s m_{qo} v_{do} + R_s m_{do} v_{qo} + L_q m_{do} v_{do} \omega_{eo} + L_d m_{qo} v_{qo} \omega_{eo} + i_{qo} m_{do} \left(R_s^2 + L_d L_q \omega_{eo}^2 \right) - i_{do} m_{qo} \left(R_s^2 + L_d L_q \omega_{eo}^2 \right)$$

$$y_1 = 2 C E_{dco}^2 L_d R_w m_{do}$$

$$y_2 = 3 E_{dco} i_{do} k_s L_d R_w \left(m_{do}^2 + m_{qo}^2 \right) - 3 L_d m_{do} R_w \left(i_{do} v_{do} + i_{qo} v_{qo} \right) + 2 E_{dco}^2 \left(R_s C m_{do} R_w + L_d \left(m_{do} + C m_{qo} R_w \omega_{eo} \right) \right)$$

$$y_3 = 3 E_{dco} k_s R_w \left(m_{do}^2 + m_{qo}^2 \right) \left(R_s i_{do} + v_{do} + i_{qo} L_d \omega_{eo} \right) + 2 E_{dco}^2 \left(R_s m_{do} + L_d m_{qo} \omega_{eo} \right) - 3 R_w \left(i_{do} v_{do} + i_{qo} v_{qo} \right) \left(R_s m_{do} + L_d m_{qo} \omega_{eo} \right)$$

$$x_4 = 2 C E_{dco}^2 R_w \left(i_{qo} L_d m_{do} - i_{do} L_q m_{qo} \right)$$

$$x_5 = 3 E_{dco} i_{do} i_{qo} k_s R_w \left(L_d - L_q \right) \left(m_{do}^2 + m_{qo}^2 \right) + 3 R_w \left(-i_{qo} L_d m_{do} + i_{do} L_q m_{qo} \right) \left(i_{do} v_{do} + i_{qo} v_{qo} \right)$$
$$+ 2 E_{dco}^2 \left(-i_{do} \left(R_s C m_{qo} R_w + L_q \left(m_{qo} - C m_{do} R_w \omega_{eo} \right) \right) + i_{qo} \left(R_s C m_{do} R_w + L_d \left(m_{do} + C m_{qo} R_w \omega_{eo} \right) \right) \right)$$

$$x_6 = 2 E_{dco}^2 \left(i_{do} \left(-R_s m_{qo} + L_q m_{do} \omega_{eo} \right) + i_{qo} \left(R_s m_{do} + L_d m_{qo} \omega_{eo} \right) \right) + 3 E_{dco} k_s R_w \left(m_{do}^2 + m_{qo}^2 \right) \left(i_{qo} v_{do} + i_{qo}^2 L_d \omega_{eo} + i_{do} \left(-v_{qo} + i_{do} L_q \omega_{eo} \right) \right)$$
$$+ 3 R_w \left(i_{do} v_{do} + i_{qo} v_{qo} \right) \left(i_{do} \left(R_s m_{qo} - L_q m_{do} \omega_{eo} \right) - i_{qo} \left(R_s m_{do} + L_d m_{qo} \omega_{eo} \right) \right)$$

$$y_4 = 2 C E_{dco}^2 L_d R_w m_{do}$$

$$y_5 = 3 E_{dco} i_{do} k_s L_d R_w \left(m_{do}^2 + m_{qo}^2 \right) - 3 L_d m_{do} R_w \left(i_{do} v_{do} + i_{qo} v_{qo} \right) + 2 E_{dco}^2 \left(R_s C m_{do} R_w + L_d \left(m_{do} + C m_{qo} R_w \omega_{eo} \right) \right)$$

$$y_6 = 3 E_{dco} k_s R_w \left(m_{do}^2 + m_{qo}^2 \right) \left(R_s i_{do} + v_{do} + i_{qo} L_d \omega_{eo} \right) + 2 E_{dco}^2 \left(R_s m_{do} + L_d m_{qo} \omega_{eo} \right) - 3 R_w \left(i_{do} v_{do} + i_{qo} v_{qo} \right) \left(R_s m_{do} + L_d m_{qo} \omega_{eo} \right)$$

09/25/2018